A combined approach for analysing evolutionary power spectrums of track-soil system under moving random loads

Y. Zhao [a], L. T. Si [a], H. Ouyang [b]

[a] *State Key Laboratory of Structural Analysis for Industrial Equipment, Faculty of Vehicle Engineering and Mechanics, Dalian University of Technology, Dalian 116023, PR China*

[b] *School of Engineering, University of Liverpool, The Quadrangle, Liverpool L69 3GH, UK*

Abstract

The pseudo excitation method combined with the integral transform method (PEM-ITM) is presented for investigating the ground vibration of a coupled track-soil system induced by moving random loads. In the track model, the rail, sleepers, rail pads and ballast are modelled as an infinite Euler beam, discretely distributed masses, discretely distributed vertical springs and a viscoelastic layer, respectively. The soil is regarded as a homogenous isotropic half-space and coupled with the track using the boundary condition at the surface of the ground. By introducing a pseudo-excitation the random vibration analysis of the coupled system is converted into a harmonic analysis. The analytical form of evolutionary power spectral density (EPSD) responses of the simplified coupled track-soil system of subjected to a random moving load is derived in the frequency/wavenumber domain by PEM-ITM. In the numerical examples, the effects of different parameters, such as the moving speed, the soil properties and the coherence of moving loads, on the ground response are investigated.

Key words: track-soil system; moving random loads; evolutionary power spectrum; pseudo-excitation method; integral transform method; vibration transmission

1. Introduction

With high-speed trains becoming increasingly popular and freight trains becoming increasingly heavier, the environmental vibration induced by trains has received considerable attention in the last few decades [1,2]. The vibration propagates from the track into the subsoil and enters buildings via the ground, and it can seriously affect the working of sensitive equipment and human comfort. In the view of spectrums, the excitation induced by a travelling train to the ground can be divided into quasi-static part and dynamic part. The quasi-static part arises from the weight of the train and the dynamic excitation is related to dynamic train-track interaction. However, due to track irregularities and other uncertainties, the dynamic excitation is somehow random, which leads to ground vibration with wide frequency spectrums.

There are plenty of research works for solving the deterministic problems of ground vibration induced by moving static or dynamic loads. For the problem of a half-space subjected to a moving point load, Fryba [3] investigated the steady-state response, and Alabi [4] considered an oblique load. Krylov [5] studied ground vibration induced by trains, in which the total distribution of forces along the track is proportional to the track deflection under the axle load. Takemiya [6] took account of the dynamic nature of the train loads, and in his solutions, the moving loads of specific frequency contents were investigated. Gunaratne [7] derived the deformations of a layered half-space subjected to a moving strip load. Considering a harmonic load moving along an elastic layer, Dieterman and Metrikine [8] derived the critical speed of wave propagation in the layer. Lefeuve-Mesgouez [9] investigated the transmission of ground vibrations induced by moving harmonic strip or rectangular loads. Jones et al. [10] studied ground vibrations induced by a fixed or moving harmonic load harmonic load in a rectangular spatial distribution. Bierer and Bode [11] investigated ground motion excited by moving harmonic loads distributed uniformly over a rectangular area. Using a layered half-space coupled with a track structure under a fixed or moving harmonic load, Sheng et al. [12] studied the vibration propagation in the ground. Hung and Yang [13] analysed the response of a half-space subjected to moving loads including a moving point load, a uniformly or elastically distributed wheel load, which is constant or harmonic in time. Koziol et al. [14] studied the surface vibration induced by a harmonic point load moving along an infinitely long beam embedded in a viscous elastic layer.

The above-mentioned authors provide numerous methods to evaluate ground vibrations and their work is very useful for further study. References [15-17] showed that a quasi-static excitation was only suitable for predicting the ground response in the immediate vicinity of the track, but unsuitable for the response a further field, which is dominated by the dynamic part. However, in rail transportation systems, the excitation to the ground is somehow random due to wheel and rail roughness, wheel-flats and other uncertainties. So the vibration at any specific locations induced by moving trains is a non-stationary random process. Taking the excitation to the ground as constant or harmonic is not adequate. Actually, the wide frequency spectrum of the excitation must be considered.

Hunt [18] presented an analytical solution to for the power spectrum of ground vibration due to traffic loads taken as a stationary random process. Sun and Greenberg [19] presented a generalized method to solve the problem of a linear system subjected to moving excitations, in which a method named follow-up spectral analysis procedure was introduced to overcome the difficulty that the dynamic response of the linear system was a non-stationary process. Using a two-dimensional model with a point load moving along a beam embedded in a layer, Metrikine and Vrouwenvelder [20] studied the steady-state ground surface vibration. The response induced by a constant or harmonic load and a stationary random load was studied, in which the random problem was solved by Monte Carlo method and the random load was represented by a white noise. Paolucci et al. [21] numerically simulated the ground vibration induced by a series of wheel forces, and they concluded that the frequency range up to 10Hz contained most of the information regarding possible harmful effects of vibrations on buildings and humans.

Sheng et al. [22] investigated train-excited ground vibration considering vertical track irregularities, and computed the dynamic wheel–rail interaction forces and the displacement power spectra of the track and the ground surface using receptance method. Lai et al. [23] assessed the vibration impact induced by a train running in a tunnel, in which the effect of rail roughness on the load spectrum was represented by an empirical formula. Using the pseudo-excitation method [24], Lu et al. [25] studied the random ground response induced by moving random loads. Lombaert et al. [26] built a numerical model of free field traffic-induced vibration during the passage of a vehicle on an uneven road and derived the transfer function between the source and the receiver.

The above mentioned researches on ground vibration induced by moving loads have greatly advanced the progress in the field of traffic-induced environmental vibration. However, there is still much work to be done to evaluate the statistical characteristics of vibration when considering random characteristics of input loads. Due to the movement of loads, one of the major difficulties is that the ground response of the observation point has a nonstationary random vibration characteristic, even though assuming that the stochastic load is a stationary stochastic process. In addition, considering the coherence properties generated by the multiple moving random loads, the superposition and cancellation of the ground vibrations are also difficult to deal with. The double-frequency spectral model and frequency-time spectral model are two mathematical structures of nonstationary random processes [27] and are also the starting point for the random vibrational analysis of linear systems. The physical concept of the double-frequency spectrum is not easy to explain and is limited in the practical application. The frequency-time spectrum (or evolutionary spectrum) proposed by Priestley contains the concept of instantaneous power and a more intuitive physical meaning. It has a good advantage to evaluate the statistical characteristics of environmental vibration based on the evolutionary spectrum concept. For linear time-invariant systems subject to nonstationary random loads, the pseudo excitation method transforms the nonstationary random vibration analysis into the usual transient response analysis, and combined with the finite element method has been effectively applied to the seismic analysis of long-span bridges , In [28], Peng et al. combine probability density evolution method with the efficient representation of stochastic processes to implement stochastic dynamic response analysis of multi-degree-of-freedom systems subjected to stochastic excitations.

In this paper, to analyse the nonstationary random vibration of the track-soil system induced by moving random loads, the pseudo excitation method combined with the integral transform method (PEM-ITM) is presented. The evolutionary power spectrum of the nonstationary random vibration of the ground is investigated by the proposed method. The effects of different parameters, such as the moving speed, the position of observation point, the soil properties and the coherence of moving loads, on the ground response mechanism are further studied. The organization of the paper is as follows. In section 2, the basic model of track-soil system and governing equations of motion are provided. In Section 3, integral transforms are used as the mean to solve the governing equations of the track-soil system, and the analytic expression of the evolutionary power spectrum of the nonstationary random vibration response is derived by the PEM-ITM. In Section 4, a parametric study on responses induced by moving random loads is made, and some dynamic phenomena of ground vibration transmission are discussed. Conclusions are given in section 5.

2. Model and governing equations

The system considered herein, shown in Fig. 1, consists of a homogenous isotropic viscoelastic half-space and a track-soil structure. The infinite track is aligned in the x direction and has a contact width $2l$ with the ground. The rail is regarded as a single infinite Euler beam with bending stiffness EI and mass ρ_{R} per unit length. The sleepers are modelled as a distributed mass m_{S} per uint length of track. The rail pads are represented by a distributed vertical spring stiffness k_{P} between the rail and the sleepers. The ballast is modelled as a viscoelastic layer with a width $2l$ and a mass per unit length m_{B}. For the ballast layer, only the vertical stiffness k_{B} is taken into account. Furthermore, the contact forces between the ballast and the ground are assumed to be normal to the ground surface and uniformly distributed over the width of the track. The damping properties of all of these track components are accounted for by using complex stiffness parameters. Now the problem of the system subjected to a moving random load is studied.

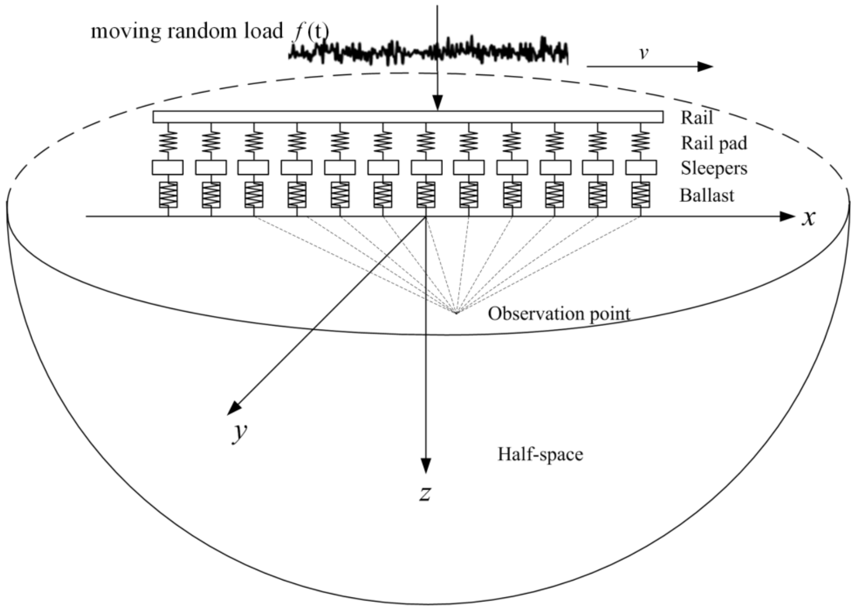

Fig.1. Model of track-soil structure under a moving random load

The vertical displacements of the rail beam, the sleepers and the ground surface are denoted by, respectively, $w_{\mathrm{R}}(x,t)$, $w_{\mathrm{S}}(x,t)$ and $w_{\mathrm{G}}(x,t)$. Similarly, the forces at the rail/sleeper, sleeper/ballast and ballast/ground interfaces are denoted by $F_{\mathrm{RS}}(x,t)$, $F_{\mathrm{SB}}(x,t)$ and $F_{\mathrm{BG}}(x,t)$.

The vertical motions of the structure are expressed by differential equations as follows. For the rail beam the differential equation of motion can be written as

$$EI\frac{\partial^4 w_{\mathrm{R}}(x,t)}{\partial x^4}+\rho_{\mathrm{R}}\frac{\partial^2 w_{\mathrm{R}}(x,t)}{\partial t^2}+F_{\mathrm{RS}}(x,t)=f(t)\delta(x-vt) \tag{1}$$

where $\delta(\cdot)$ is the Dirac-delta function, the time varying function $f(t)$ is characterized as a stationary random process and its power spectral density is represented by $S_f(\omega)$.

The interaction force $F_{\mathrm{RS}}(x,t)$ between the rail and the sleeper is

$$F_{\mathrm{RS}}(x,t)=k_{\mathrm{P}}[w_{\mathrm{R}}(x,t)-w_{\mathrm{S}}(x,t)] \tag{2}$$

For the sleeper mass, the differential equation of motion is

$$m_{\mathrm{S}}\frac{\partial^2 w_{\mathrm{S}}(x,t)}{\partial t^2}+F_{\mathrm{SB}}(x,t)=F_{\mathrm{RS}}(x,t) \tag{3}$$

and for the ballast layer a linear spring stiffness with a consistent mass approximation is used so that

$$\frac{m_{\mathrm{B}}}{6}\begin{bmatrix}2 & 1\\1 & 2\end{bmatrix}\begin{Bmatrix}\dfrac{\partial^2 w_{\mathrm{S}}(x,t)}{\partial t^2}\\\dfrac{\partial^2 w_{\mathrm{G}}(x,t)}{\partial t^2}\end{Bmatrix}+k_{\mathrm{B}}\begin{bmatrix}1 & -1\\-1 & 1\end{bmatrix}\begin{Bmatrix}w_{\mathrm{S}}(x,t)\\w_{\mathrm{G}}(x,t)\end{Bmatrix}+\begin{Bmatrix}-F_{\mathrm{SB}}(x,t)\\F_{\mathrm{BG}}(x,t)\end{Bmatrix}=\mathbf{0} \tag{4}$$

Considering the interaction force is uniformly distributed over the width of the track, the boundary condition on the surface of the ground is represented by

$$\sigma_{zz}(x,y,z,t)=-\frac{F_{\mathrm{BG}}\mathrm{H}(l^2-y^2)}{2l},\tau_{zx}(x,y,z,t)=0,\tau_{zy}(x,y,z,t)=0 \tag{5}$$

where $\mathrm{H}(\cdot)$ is the step function which restricts the interaction force within the width of the track, σ_{zz} is the normal stress, τ_{zx} and τ_{zy} are the shear stresses.

Meanwhile, by ignoring the body force of the weight, the differential equation of the ground is

$$(\lambda+\mu)\nabla(\nabla\cdot\mathbf{u})+\mu\nabla^2\mathbf{u}=\rho\frac{\partial^2\mathbf{u}}{\partial t^2} \tag{6}$$

where ∇ is the Gradient operator and ∇^2 is the Laplace operator, ρ is the mass density of the soil, λ and μ are Lamé's constants derived from its Young's modulus E and Poisson's ratio ν, and $\mathbf{u}=\{\mathrm{u}(x,y,z,t),v(x,y,z,t),w(x,y,z,t)\}$ is the displacement vector.

3. Analytical solutions

3.1. General solution to decouple governing equations

Throughout this paper, the triple Fourier transform and its inverse are defined as follows

$$\begin{aligned}\hat{\hat{\hat{f}}}(k_x,k_y,\beta)&=\int_{-\infty}^{\infty}\int_{-\infty}^{\infty}\int_{-\infty}^{\infty}f(x,y,t)\mathrm{e}^{-\mathrm{i}k_x x}\mathrm{e}^{-\mathrm{i}k_y y}\mathrm{e}^{-\mathrm{i}\beta t}\,\mathrm{d}x\mathrm{d}y\mathrm{d}t\\f(x,y,t)&=\frac{1}{8\pi^3}\int_{-\infty}^{\infty}\int_{-\infty}^{\infty}\int_{-\infty}^{\infty}\hat{\hat{\hat{f}}}(k_x,k_y,\beta)\mathrm{e}^{\mathrm{i}k_x x}\mathrm{e}^{\mathrm{i}k_y y}\mathrm{e}^{\mathrm{i}\beta t}\,\mathrm{d}k_x\mathrm{d}k_y\mathrm{d}\beta\end{aligned} \tag{7}$$

By applying a double Fourier transform ($x\to k_x, t\to\beta$) to Eqs. (1) - (4), one can obtain algebraic equations in $\hat{\hat{w}}_{\mathrm{R}}(k_x,\beta)$, $\hat{\hat{w}}_{\mathrm{S}}(k_x,\beta)$ and $\hat{\hat{w}}_{\mathrm{G}}(k_x,\beta)$ in the combined frequency and wavenumber domain as

$$\begin{bmatrix} K_{11} & K_{12} & K_{13} \\ K_{21} & K_{22} & K_{23} \\ K_{31} & K_{32} & K_{33} \end{bmatrix} \begin{Bmatrix} \hat{\hat{w}}_{\mathrm{R}} \\ \hat{\hat{w}}_{\mathrm{S}} \\ \hat{\hat{w}}_{\mathrm{G}} \end{Bmatrix} = \begin{Bmatrix} \hat{\hat{F}}_{\mathrm{E}} \\ 0 \\ \hat{\hat{F}}_{\mathrm{BG}} \end{Bmatrix} \tag{8}$$

in which the elements of the matrix are $K_{11} = EIk_x^4 - \rho_{\mathrm{R}}\beta^2 + k_{\mathrm{P}}$, $K_{12} = -k_{\mathrm{P}}$, $K_{13} = 0$, $K_{21} = -K_{12}$, $K_{22} = \left(\frac{m_{\mathrm{B}}}{3} + m_{\mathrm{S}}\right)\beta^2 - (k_{\mathrm{B}} + k_{\mathrm{P}})$, $K_{23} = \frac{m_{\mathrm{B}}}{6}\beta^2 + k_{\mathrm{B}}$, $K_{31} = 0$, $K_{32} = K_{23}$, $K_{33} = \frac{m_{\mathrm{B}}}{3}\beta^2 - k_{\mathrm{B}}$.

In the combined frequency and wavenumber domain, the load applied on the track has the form of

$$\hat{\hat{F}}_{\mathrm{E}} = \hat{f}(\beta + k_x v) \tag{9}$$

with $\hat{\hat{F}}_{\mathrm{BG}}$ unknown.

In Eq. (8), $\hat{\hat{w}}_{\mathrm{R}}$ and $\hat{\hat{w}}_{\mathrm{S}}$ can be expressed by $\hat{\hat{w}}_{\mathrm{G}}$ and $\hat{\hat{F}}_{\mathrm{E}}$ as

$$\hat{\hat{w}}_{\mathrm{R}} = \frac{K_{22}\hat{\hat{F}}_{\mathrm{E}} + K_{12}K_{23}\hat{\hat{w}}_{\mathrm{G}}}{K_{12}^2 + K_{11}K_{22}} \tag{10}$$

$$\hat{\hat{w}}_{\mathrm{S}} = \frac{K_{12}\hat{\hat{F}}_{\mathrm{E}} - K_{11}K_{23}\hat{\hat{w}}_{\mathrm{G}}}{K_{12}^2 + K_{11}K_{22}} \tag{11}$$

Furthermore, the relation between the vertical force and the displacement on the surface of the ground is

$$\hat{\hat{F}}_{\mathrm{BG}} = \bar{K}_1\hat{\hat{w}}_{\mathrm{G}} + \bar{K}_2\hat{\hat{F}}_{\mathrm{E}} \tag{12}$$

where

$$\bar{K}_1 = \frac{K_{12}^2K_{33} + K_{11}K_{22}K_{33} - K_{11}K_{23}^2}{K_{12}^2 + K_{11}K_{22}}, \bar{K}_2 = \frac{K_{12}K_{23}}{K_{12}^2 + K_{11}K_{22}} \tag{13}$$

By applying a triple Fourier transform to Eq. (5), the stresses on the surface of the ground are transformed as

$$\hat{\hat{\hat{\sigma}}}_{zz} = -\hat{\hat{F}}_{\mathrm{BG}}\frac{\sin(k_y l)}{k_y l}, \hat{\hat{\hat{\tau}}}_{zx} = 0, \hat{\hat{\hat{\tau}}}_{zy} = 0 \tag{14}$$

If Eq. (12) is substituted into Eq. (14), it can be seen that this stresses are expressed as a function of displacement $\hat{\hat{w}}_{\mathrm{G}}$ and external load $\hat{\hat{F}}_{\mathrm{E}}$. Next the motion of the ground is studied.

According to Helmholtz decomposition of a vector field, the solution of Eq. (6) is given as

$$\mathbf{u} = \nabla\phi + \nabla \times \boldsymbol{\psi} \tag{15}$$

where ϕ is a scalar potential, and $\boldsymbol{\psi} = [\psi_1, \psi_2, \psi_3]^{\mathrm{T}}$ is a vector potential in which $\psi_3 = 0$. Expanding Eq. (15) leads to the displacement components

$$\begin{gathered} u = \frac{\partial\phi}{\partial x} - \frac{\partial\psi_2}{\partial z} \\ v = \frac{\partial\phi}{\partial y} + \frac{\partial\psi_1}{\partial z} \\ w = \frac{\partial\phi}{\partial z} + \frac{\partial\psi_2}{\partial x} - \frac{\partial\psi_1}{\partial y} \end{gathered} \tag{16}$$

Expressed by displacement components, the stress components are derived as

$$\begin{gathered} \sigma_{zz} = \left(\lambda\nabla^2 + 2\mu\frac{\partial^2}{\partial z^2}\right)\phi + 2\mu\left(\frac{\partial^2\psi_2}{\partial x\partial z} - \frac{\partial^2\psi_1}{\partial y\,\partial z}\right) \\ \tau_{zx} = \mu\left(2\frac{\partial^2\phi}{\partial x\,\partial z} - \frac{\partial^2\psi_1}{\partial x\,\partial y} + \frac{\partial^2\psi_2}{\partial \chi^2} - \frac{\partial^2\psi_2}{\partial z^2}\right) \\ \tau_{zy} = \mu\left(2\frac{\partial^2\phi}{\partial y\,\partial z} - \frac{\partial^2\psi_1}{\partial y^2} + \frac{\partial^2\psi_1}{\partial z^2} + \frac{\partial^2\psi_2}{\partial x\,\partial y}\right) \end{gathered} \tag{17}$$

Substituting Eq. (15) into Eq. (6) yields the wave equations below

$$\nabla^2\phi = \frac{1}{c_{\mathrm{D}}^2}\frac{\partial^2\phi}{\partial t^2}, \nabla^2\boldsymbol{\psi} = \frac{1}{c_{\mathrm{S}}^2}\frac{\partial^2\boldsymbol{\psi}}{\partial t^2} \tag{18}$$

in which $c_{\mathrm{D}} = \sqrt{(\lambda + 2\mu)/\,\rho}$ and $c_{\mathrm{S}} = \sqrt{\mu/\rho}$ are the velocities of the dilatational waves and the shear waves, respectively.

By applying a triple Fourier transform, the partial differential Eq. (18) is changed into ordinary differential equations

$$\frac{\partial\hat{\hat{\hat{\phi}}}}{\partial z^2} - E_{\mathrm{D}}^2\hat{\hat{\hat{\phi}}} = 0, \frac{\partial\hat{\hat{\hat{\boldsymbol{\psi}}}}}{\partial z^2} - E_{\mathrm{S}}^2\hat{\hat{\hat{\boldsymbol{\psi}}}} = 0 \tag{19}$$

where $E_{\mathrm{D,S}}^2 = k_x^2 + k_y^2 - k_{\mathrm{D,S}}^2$, $k_{\mathrm{D,S}} = \beta/c_{\mathrm{D,S}}$.

The general solutions of Eq. (19) are

$$\hat{\hat{\hat{\phi}}} = C_1\mathrm{e}^{-E_{\mathrm{D}}z}, \hat{\hat{\hat{\psi}}}_1 = C_2\mathrm{e}^{-E_{\mathrm{S}}z}, \hat{\hat{\hat{\psi}}}_2 = C_3\mathrm{e}^{-E_{\mathrm{S}}z} \tag{20}$$

By applying a triple Fourier transform to Eq. (17) and substituting Eq. (20) into it, the stress components have the form of

$$\begin{Bmatrix} \hat{\hat{\hat{\sigma}}}_{zz} \\ \hat{\hat{\hat{\tau}}}_{zx} \\ \hat{\hat{\hat{\tau}}}_{zy} \end{Bmatrix} = \mathbf{TQ} \begin{Bmatrix} C_1 \\ C_2 \\ C_3 \end{Bmatrix} \tag{21}$$

in which $\mathbf{T} = \mu \begin{bmatrix} 2\left(k_x^2 + k_y^2\right) - k_\mathrm{S}^2 & 2\mathrm{i}k_y E_\mathrm{S} & -2\mathrm{i}k_x E_\mathrm{S} \\ -2\mathrm{i}k_x E_\mathrm{D} & k_x k_y & -(k_x^2 + E_\mathrm{S}^2) \\ -2\mathrm{i}k_y E_\mathrm{D} & \left(k_y^2 + E_\mathrm{S}^2\right) & -k_x k_y \end{bmatrix}$ and $\mathbf{Q} = \mathrm{diag}(\mathrm{e}^{-E_\mathrm{D}z} \mathrm{e}^{-E_\mathrm{S}z} e^{-E_\mathrm{S}z})$.

Notice that on the surface of the half-space, $\hat{\hat{\hat{\tau}}}_{zx} = \hat{\hat{\hat{\tau}}}_{zy} = 0$, thus constants C_1, C_2 and C_3 can be determined as

$$\begin{Bmatrix} C_1 \\ C_2 \\ C_3 \end{Bmatrix} = \frac{\hat{\hat{\hat{\sigma}}}_{zz}}{\mu\Delta} \begin{Bmatrix} 2\left(k_x^2 + k_y^2\right) - k_\mathrm{S}^2 \\ 2\mathrm{i}k_y E_\mathrm{D} \\ -2\mathrm{i}k_x E_\mathrm{D} \end{Bmatrix} \tag{22}$$

in which $\Delta = \left(k_x^2 + k_y^2 + E_\mathrm{S}^2\right)^2 - 4E_\mathrm{D}E_\mathrm{S}\left(k_x^2 + k_y^2\right)$.

Thus the relationship of C_1, C_2 and C_3 is

$$C_2 = \frac{2\mathrm{i}k_y E_\mathrm{D}}{2\left(k_x^2 + k_y^2\right) - k_\mathrm{S}^2} C_1, C_3 = -\frac{2\mathrm{i}k_x E_\mathrm{D}}{2\left(k_x^2 + k_y^2\right) - k_\mathrm{S}^2} C_1 \tag{23}$$

By applying a triple Fourier transform to Eq. (16) and introducing Eq. (20) into it, the vertical displacement is derived as

$$\hat{\hat{\hat{w}}} = -C_1 E_\mathrm{D} \mathrm{e}^{-E_\mathrm{D}z} - \mathrm{i}k_y C_2 \mathrm{e}^{-E_\mathrm{S}z} + \mathrm{i}k_x C_3 \mathrm{e}^{-E_\mathrm{S}z} \tag{24}$$

The inverse transform of Eq. (24) on k_y is

$$\hat{\hat{w}}(k_x, y, z, \beta) = \frac{1}{2\pi} \int_{-\infty}^{\infty} \left(-C_1 E_\mathrm{D} \mathrm{e}^{-E_\mathrm{D}z} - \mathrm{i}k_y C_2 \mathrm{e}^{-E_\mathrm{S}z} + \mathrm{i}k_x C_3 \mathrm{e}^{-E_\mathrm{S}z}\right) \mathrm{e}^{\mathrm{i}k_y y} \mathrm{d}k_y \tag{25}$$

Thus, the vertical displacement at $y = 0$ on the half-space surface is

$$\hat{\hat{w}}(k_x, 0,0, \beta) = \frac{1}{2\pi} \int_{-\infty}^{\infty} \left(-C_1 E_\mathrm{D} - \mathrm{i}k_y C_2 + \mathrm{i}k_x C_3\right) \mathrm{d}k_y \tag{26}$$

Using Eq. (14) and Eq. (22), the coefficient C_1 is calculated as

$$C_1 = -\frac{\left[2\left(k_x^2 + k_y^2\right) - k_\mathrm{S}^2\right]}{\mu\Delta} \frac{\sin\left(k_y l\right)}{k_y l} \hat{\hat{F}}_\mathrm{BG}(k_x, \beta) \tag{27}$$

Further, using Eq. (23) C_2 and C_3 are given as

$$C_2 = -\frac{2\mathrm{i}k_y E_\mathrm{D}}{\mu\Delta} \frac{\sin\left(k_y l\right)}{k_y l} \hat{\hat{F}}_\mathrm{BG}(k_x, \beta),\ C_3 = \frac{2\mathrm{i}k_x E_\mathrm{D}}{\mu\Delta} \frac{\sin\left(k_y l\right)}{k_y l} \hat{\hat{F}}_\mathrm{BG}(k_x, \beta) \tag{28}$$

Substituting Eqs. (27) - (28) into Eq. (26) and using displacement continuity conditions of the track and ground yield

$$\begin{aligned}\hat{\hat{w}}_{\mathrm{G}}(k_x,\beta) &= \hat{\hat{w}}(k_x,0,0,\beta) = -H_1(k_x,\beta)\hat{\hat{F}}_{\mathrm{BG}}(k_x,\beta)\\ H_1(k_x,\beta) &= \frac{1}{2\pi}\int_{-\infty}^{\infty}\frac{1}{\mu\Delta}\frac{\sin(k_y l)}{k_y l}E_{\mathrm{D}}k_{\mathrm{S}}^2\mathrm{d}k_y\end{aligned}\tag{29}$$

Further, using Eq. (12) and Eq. (29) $\hat{\hat{w}}_{\mathrm{G}}(k_x,\beta)$ can be obtained as

$$\begin{aligned}\hat{\hat{w}}_{\mathrm{G}}(k_x,\beta) &= H_2(k_x,\beta)\hat{\hat{F}}_{\mathrm{E}}\\ H_2(k_x,\beta) &= \frac{-H_1(k_x,\beta)\bar{K}_2}{1+\bar{K}_1H_1(k_x,\beta)}\hat{\hat{F}}_{\mathrm{E}}\end{aligned}\tag{30}$$

Substituting $\hat{\hat{w}}_{\mathrm{G}}$ into Eq. (10) $\hat{\hat{w}}_{\mathrm{R}}$ results in

$$\hat{\hat{w}}_{\mathrm{R}}(k_x,\beta) = \frac{K_{22}+K_{12}K_{23}H_2(k_x,\beta)}{K_{12}^2+K_{11}K_{22}}\hat{\hat{F}}_{\mathrm{E}}(k_x,\beta)\tag{31}$$

The inverse transform of Eq. (31) on k_y is

$$\hat{w}_{\mathrm{R}}(x,\beta) = \frac{1}{2\pi}\int_{-\infty}^{\infty}\frac{K_{22}+K_{12}K_{23}H_2(k_x,\beta)}{K_{12}^2+K_{11}K_{22}}\hat{\hat{F}}_{\mathrm{E}}(k_x,\beta)\mathrm{e}^{\mathrm{i}k_x x}\mathrm{d}k_x\tag{32}$$

By substituting C_1, C_2 and C_3 into Eq. (25) one can get the vertical displacement in the frequency/wavenumber domain as

$$\begin{aligned}\hat{\hat{w}}(k_x,y,0,\beta) &= -H_3(k_x,y,\beta)\hat{\hat{F}}_{\mathrm{E}}(k_x,\beta)\\ H_3(k_x,y,\beta) &= \frac{1}{2\pi}\left(\int_{-\infty}^{\infty}\frac{1}{\mu\Delta}\frac{\sin(k_y l)}{k_y l}E_{\mathrm{D}}k_{\mathrm{S}}^2\mathrm{e}^{\mathrm{i}k_y y}\mathrm{d}k_y\right)\frac{\bar{K}_2}{1+\bar{K}_1H_1(k_x,\beta)}\end{aligned}\tag{33}$$

Applying the inverse transform to Eq. (33) leads to the vertical displacement in the physical domain as

$$\begin{aligned}w(x,y,0,t) &= \frac{1}{4\pi^2}\int_{-\infty}^{\infty}\int_{-\infty}^{\infty}\hat{\hat{w}}(k_x,y,0,\beta)\mathrm{e}^{\mathrm{i}k_x x}\mathrm{e}^{\mathrm{i}\beta t}\mathrm{d}k_x\mathrm{d}\beta\\ &= \frac{1}{4\pi^2}\int_{-\infty}^{\infty}\int_{-\infty}^{\infty}-H_3(k_x,y,\beta)\hat{\hat{F}}_{\mathrm{E}}(k_x,\beta)\mathrm{e}^{\mathrm{i}k_x x}\mathrm{e}^{\mathrm{i}\beta t}\mathrm{d}k_x\mathrm{d}\beta\end{aligned}\tag{34}$$

So far the general solution to decouple the governing equations of the track-soil is presented. If the time varying function $f(t)$ is in a harmonic form or is constant, one can use the solution to obtain the deterministic response. However, due to the existence of track irregularities, it is more realistic to assume $f(t)$ as a stochastic process. Therefore the response has to be calculated according to the probability and statistics theory, which is given in the following section.

3.2. Non-stationary random vibration analysis

The pseudo-excitation method [28-31] is a well-established algorithm for analysing the responses of linear time-invariant systems under stationary or non-stationary random excitations. It has been widely used in earthquake engineering fields. Hence the pseudo-excitation method is introduced in this part.

A Green's function can be used to characterize the dynamic properties of a linear system. The Green's function $\mathbf{G}(\mathbf{x}, t; \boldsymbol{\xi}, \tau)$ represents the dynamic response at location $\mathbf{x}$ and time t when the system is subjected to a vertical impulse at location $\boldsymbol{\xi}$ and time τ. For a time-independent system, the Green's function degenerates to $\mathbf{G}(\mathbf{x} - \boldsymbol{\xi}, t - \tau)$. Assume that $f(t)$ is a stationary random load moving along direction $\mathbf{n}$ at constant speed v, and $\mathbf{D}$ is the domain occupied by the system. According to the principle of superposition, the displacement of the system can be written as

$$\mathbf{u}(\mathbf{x}, t) = \int_0^t \int_{\mathbf{D}} \mathbf{G}(\mathbf{x} - \boldsymbol{\xi} - \mathbf{n}v\tau, t - \tau) \cdot f(\tau) \mathrm{d}\boldsymbol{\xi} \, \mathrm{d}\tau \tag{35}$$

Applying expectation operator $E[\cdot]$ to $\mathbf{u}(\mathbf{x}, t)$ generates its correlation function

$$\begin{aligned} \mathbf{R}_{\mathbf{u}}(\mathbf{x}; t_1, t_2) &= E[\mathbf{u}(\mathbf{x}, t_1)\mathbf{u}^{\mathrm{T}}(\mathbf{x}, t_2)] \\ &= \int_0^{t_1} \int_0^{t_2} \mathbf{h}(\mathbf{x}; t_1, \tau_1) \cdot \mathbf{h}^{\mathrm{T}}(\mathbf{x}; t_2, \tau_2) R_f(\Delta\tau) \mathrm{d}\tau_1 \, \mathrm{d}\tau_2 \end{aligned} \tag{36}$$

where

$$\mathbf{h}(\mathbf{x}; t, \tau) = \int_{\mathbf{D}} \mathbf{G}(\mathbf{x} - \boldsymbol{\xi} - \mathbf{n}v\tau, t - \tau) \mathrm{d}\boldsymbol{\xi} \tag{37}$$

$\Delta\tau = \tau_2 - \tau_1$ and $R_f(\Delta\tau)$ is the autocorrelation function of the load. According to the Wiener-Khintchine theorem, $R_f(\Delta\tau)$ can be expressed by the power spectral densities (PSD) $S_f(\omega)$ as

$$E[f(\tau_1)f(\tau_2)] = R_f(\Delta\tau) = \int_{-\infty}^{\infty} S_f(\omega) \mathrm{e}^{\mathrm{i}\omega(\tau_2 - \tau_1)} \, \mathrm{d}\omega \tag{38}$$

Where $S_f(\omega)$ reflects the energy distribution of a stationary random process in the frequency domain. Substituting Eq. (38) into Eq. (36), the correlation function can be written as

$$\mathbf{R}_{\mathbf{u}}(\mathbf{x}; t_1, t_2) = \int_{-\infty}^{\infty} S_f(\omega) \mathbf{I}^*(\mathbf{x}; \omega, t_1) \mathbf{I}^{\mathrm{T}}(\mathbf{x}; \omega, t_2) \, \mathrm{d}\omega \tag{39}$$

$$\mathbf{I}(\mathbf{x};\omega,t)=\int_0^t \mathbf{h}(\mathbf{x};t,\tau)\mathrm{e}^{\mathrm{i}\omega\tau}\mathrm{d}\tau \tag{40}$$

where superscript ‘*’ denotes a complex conjugate.

The time-dependent variance can be obtained by letting $t_1=t_2=t$ in Eq. (39), as

$$\mathbf{R_u}(\mathbf{x};t)=\sigma_u^2(\mathbf{x};t)=\int_{-\infty}^{\infty} S_p(\omega)\mathbf{I}^*(\mathbf{x};\omega,t)\mathbf{I}^{\mathrm{T}}(\mathbf{x};\omega,t)\,\mathrm{d}\omega \tag{41}$$

Here $\sigma_u(\mathbf{x};t)$ is the standard deviation. Obviously, the integrand in Eq. (41) is the PSD of the response, which has the non-stationary property of

$$\mathbf{S_u}(\mathbf{x},\omega,t)=S_f(\omega)\mathbf{I}^*(\mathbf{x};\omega,t)\mathbf{I}^{\mathrm{T}}(\mathbf{x};\omega,t) \tag{42}$$

Note that in Eq. (42) $\mathbf{I}(\mathbf{x};\omega,t)$ is the response of the system under a harmonic load $\mathrm{e}^{\mathrm{i}\omega t}$. So if a pseudo-excitation $\sqrt{S_f(\omega)}\mathrm{e}^{\mathrm{i}\omega t}$ is applied to the system, the corresponding response evolves to $\tilde{\mathbf{u}}(\mathbf{x};\omega,t)=\sqrt{S_f(\omega)}\mathbf{I}(\mathbf{x};\omega,t)$. Thus the PSD of the response can be obtained easily from

$$\mathbf{S_u}(\mathbf{x},\omega,t)=\tilde{\mathbf{u}}^*(\mathbf{x};\omega,t)\tilde{\mathbf{u}}^{\mathrm{T}}(\mathbf{x};\omega,t) \tag{43}$$

Now, the pseudo excitation method is used to analyse evolutionary power spectrum of the nonstationary random vibration of a track-soil system subjected to moving random loads. According to the PEM, the pseudo load can be constructed as

$$\tilde{f}(t)=\sqrt{S_f(\omega)}\mathrm{e}^{\mathrm{i}\omega t} \tag{44}$$

Then according to Eq. (9) the pseudo load in the frequency and wavenumber domain can be expressed as

$$\hat{\hat{\tilde{F}}}_{\mathrm{E}}=2\pi\sqrt{S_f(\omega)}\delta(\beta+k_x v-\omega) \tag{45}$$

Substituting Eq. (45) into Eq. (34) leads to

$$\tilde{w}(x,y,0,t)=\frac{\sqrt{S_f(\omega)}\mathrm{e}^{\mathrm{i}\omega t}}{2\pi}\int_{-\infty}^{\infty} H_3(k_x,y,\omega-k_x v)\mathrm{e}^{\mathrm{i}k_x(x-vt)}\mathrm{d}k_x \tag{46}$$

So the power spectral density of the vertical displacement can be computed as

$$S_w(\mathbf{x},\omega,t)=\tilde{w}^*(\mathbf{x},\omega,t)\cdot\tilde{w}(\mathbf{x},\omega,t) \tag{47}$$

Its time-dependent variance is calculated by

$$\sigma_w^2(\mathbf{x},t)=\int_{-\infty}^{\infty} S_w(\mathbf{x},\omega,t)\mathrm{d}\omega \tag{48}$$

4. Numerical examples

The parameters of the railway track are listed in Table 1 and three types of soil parameters are selected from the references, as shown in Table 2. The soil parameter A is measured at a particular British Rail site. The stiffness of soil B is slightly lower than that of soil A, while the stiffness of soil C is the lowest. Unless otherwise specified, the parameters of soil A are used for discussion and analysis. In addition, it is assumed that the random load is moving along the *x*-axis from the negative side to the positive side. For simple description, the starting time begins at a negative value, and time instant $t = 0$ is taken as the moment when the moving load passes through the origin. To obtain the response one has to evaluate the integral in equation (46), which can be simply done numerically since the integral kernel quickly vanishes as $|k_x|$ approaches infinity.

Given that there is no standard PSD data available for the moving random load at present, a band-limited white noise below is taken to represent the load's PSD:

$$S_f(\omega) = 63.66\ \mathrm{kN}^2/\mathrm{rad} \cdot \mathrm{s}, \omega \in [\pi, 100\pi] \tag{49}$$

Table 1. Parameters for the railway track

Mass of rail beam per unit length of track	$120\ \mathrm{kg} \cdot \mathrm{m}^{-1}$
Bending stiffness of rail beam	$1.26\times10^7\ \mathrm{N} \cdot \mathrm{m}^2$
Rail pad stiffness	$3.5\times10^8\ \mathrm{N} \cdot \mathrm{m}^{-2}$
Rail pad loss factor	0.15
Mass of sleepers per unit length of track	$490\ \mathrm{kg} \cdot \mathrm{m}^{-1}$
Mass of ballast per unit length of track	$1200\ \mathrm{kg} \cdot \mathrm{m}^{-1}$
Ballast stiffness per unit length of track	$3.15\times10^8\ \mathrm{N} \cdot \mathrm{m}^{-2}$
Loss factor of ballast	1.0
Contact width of railway and ground	$2.7\ \mathrm{m}$

Table 2. Soil parameters

Parameters	Soil A	Soil B	Soil C

Lamé constant: μ(Pa)	1.07×10^8	0.8×10^8	2×10^7
Mass density: $\rho(\mathrm{kg/m^3})$	1550	1250	2000
Poisson's ratio: ν	0.257	0.257	0.25
Loss factor: ξ	0.1	0.1	0.02
Rayleigh wave velocity: $c_{\mathrm{R}}(\mathrm{m/s})$	242	232	92
Shear wave velocity: $c_{\mathrm{S}}(\mathrm{m/s})$	263	252	100
Compression wave velocity: $c_{\mathrm{P}}(\mathrm{m/s})$	459	411	173.2

4.1 Different speed conditions

When the load moves along the track at the speeds of $50\,\mathrm{km/h}, 150\,\mathrm{km/h}, 250\,\mathrm{km/h}$ and $350\,\mathrm{km/h}$ respectively, the ground observation point A $(0, 0, 0)$ is selected to evaluate the vibration. Fig. 2 - Fig. 3 show the time-dependent standard deviation and the evolutionary power spectrum of the vertical displacement response at observation point A, respectively.

For observation point A, as can be seen from Fig. 2(a) - Fig. 2(d), the standard deviation curve becomes narrower with the increase of the load speed, and the peak of response does not change much: the peak value is $8.4393\times 10^{-6}\,\mathrm{m}$ when $v = 50\,\mathrm{km/h}$; the peak value is $8.4056\times 10^{-6}\,\mathrm{m}$ when $v = 150\,\mathrm{km/h}$; the peak value is $8.3559\times 10^{-6}\,\mathrm{m}$ when $v = 250\,\mathrm{km/h}$; the peak value is $8.3046\times 10^{-6}\,\mathrm{m}$ when $v = 350\,\mathrm{km/h}$. The vibration duration is relatively long for the low-speed ($v = 50\,\mathrm{km/h}$) and is symmetrical with respect to time axis $t = 0$ (Fig. 2(a)). However, the response's time at a the high speed ($v = 350\,\mathrm{km/h}$) becomes very short, and its duration after passing the origin is significantly longer than before the load passes the origin (Fig. 2(d)). The reason for this phenomenon is the Doppler effect in which the vibration frequency of the response becomes higher as the load approaches the observation point (the origin in this case) and the vibration frequency of the response becomes lower as the load moves away from the origin. At the same time, the damping of the system causes the high-frequency response component to decay faster and the low-frequency response component last longer.

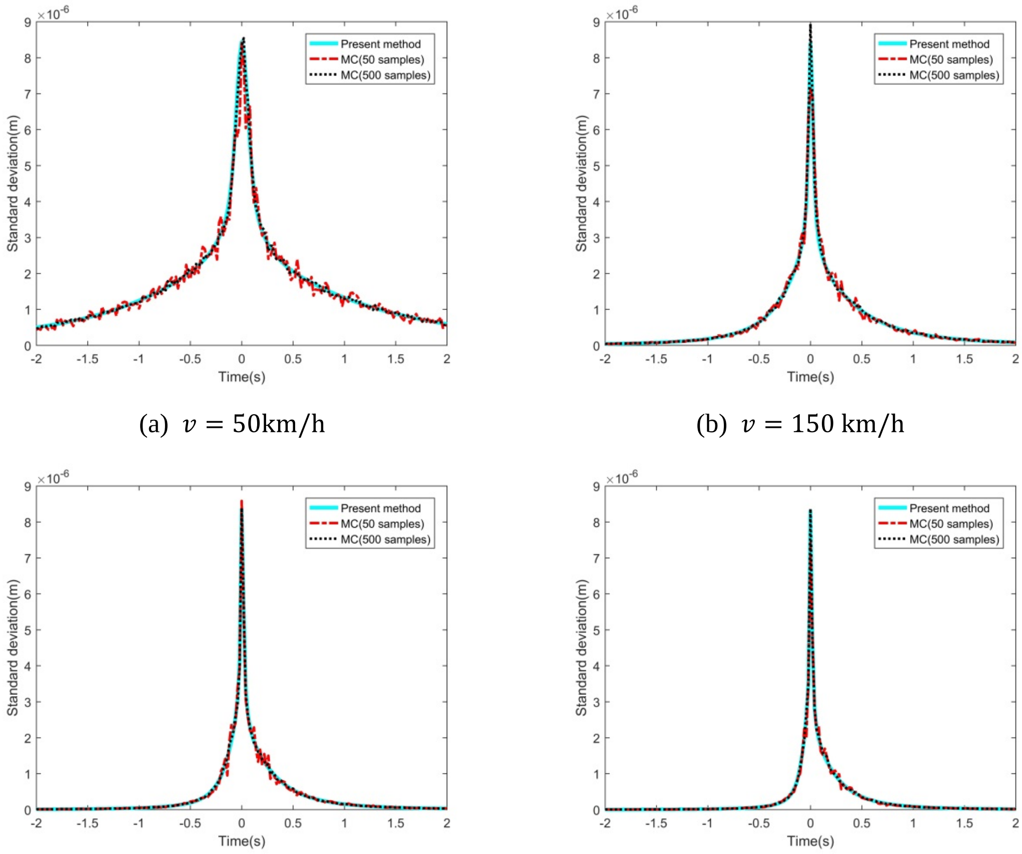

(a) $v = 50\mathrm{km/h}$ (b) $v = 150\ \mathrm{km/h}$

(c) $v = 250\ \mathrm{km/h}$ (d) $v = 350\ \mathrm{km/h}$

Fig. 2. Time-dependent standard deviation of vertical displacement at the point A (0, 0, 0) for different speeds

For the evolutionary power spectrum of the response of point A, as shown in Fig. 3(a) - Fig. 3(d), the peak of the power spectrum increases with the increasing speed: the peak value is $2.5679\times 10^{-13}\ \mathrm{m^2/rad\cdot s}$ ($v = 50\ \mathrm{km/h}$); the peak value is $2.6988\times 10^{-13}\ \mathrm{m^2/rad\cdot s}$ ($v = 150\ \mathrm{km/h}$); the peak value is $3.0180\times 10^{-13}\ \mathrm{m^2/rad\cdot s}$ ($v = 250\ \mathrm{km/h}$); the peak value is $3.6842\times 10^{-13}\ \mathrm{m^2/rad\cdot s}$ ($v = 350\ \mathrm{km/h}$). Along the time axis, the evolutionary power spectrum of the response concentrates toward the time axis $t = 0$, at which time the load passes through the observation point, and as the speed increases, the concentration becomes more pronounced. From the frequency axis, the energy of the vibration is concentrated below $250\ \mathrm{rad/s}$. At a speed of $350\ \mathrm{km/h}$, the peak appears at the frequency of $94.85\ \mathrm{rad/s}$ (Fig. 3(d)). The time-dependent standard deviation is given by the frequency-domain integral of the evolutionary power spectrum and only reflects an overall distribution of vibration (i.e., the changes in vibration amplitude over time).

However, the evolutionary power spectrum can intuitively give the time-frequency distribution of vibration.

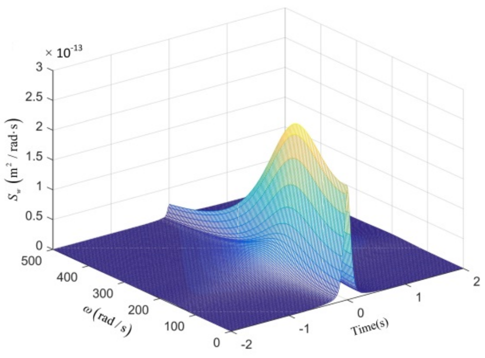

(a) $v = 50\text{km/h}$

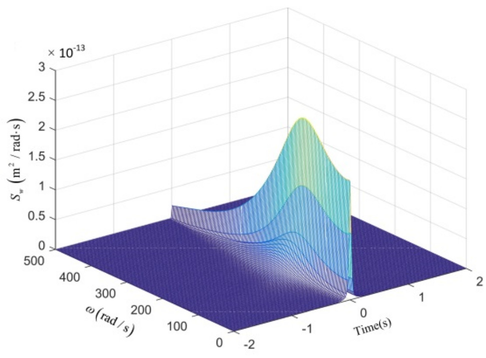

(b) $v = 150\text{ km/h}$

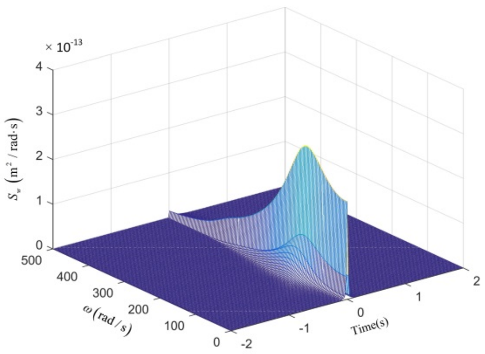

(c) $v = 250\text{ km/h}$

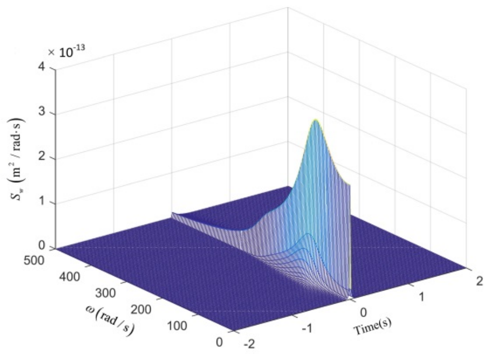

(d) $v = 350\text{ km/h}$

Fig. 3. Non-stationary evolutionary power spectrum of vertical displacement at the point A (0, 0, 0) for different speeds

In order to verify the correctness of the proposed method, the Monte Carlo (MC) method is also used to calculate the time-dependent standard deviation of the observation point. The Monte Carlo method is a general method to determine solutions of systems subjected to a random load, in which the random samples of the load can be generated and then the response to each sample load can be computed in a deterministic form, and then the statistical properties of the system can be obtained from the responses to all the samples. The samples of $f(t)$ can be generated using power spectral density $S_f(\omega)$. By harmonic series superposition method the samples are given as

$$f(t) = \sqrt{2}\sum_{k=1}^{N}\sqrt{S_f(\omega_k)\Delta\omega}\cos(\omega_k t + \phi_k) \tag{50}$$

where $S_f(\omega_k)$ is the value of $S_f(\omega)$ at the kth frequency ω_k, $\Delta\omega$ is a small regular interval of frequency and ϕ_k is the corresponding phase of ω_k and is taken as a random variable in uniformly distribution over the range of $[0, 2\pi]$.

Then, according to Eq. (9) the load in Eq. (50) can be transformed as

$$\hat{\hat{F}}_E = \sqrt{2}\pi \sum_{k=1}^{N} \sqrt{S_f(\omega_k)\Delta\omega} \left[\mathrm{e}^{\mathrm{i}\phi_k}\delta(\beta + k_x v - \omega_k) + \mathrm{e}^{-\mathrm{i}\phi_k}\delta(\beta + k_x v + \omega_k) \right] \tag{51}$$

Substituting Eq. (51) into Eq. (34), a time-domain response sample can be calculated. By generating different excitation samples and repeating the above analysis steps, multiple time-domain response samples can be obtained. Finally, the probability characteristics of the random responses can be obtained by the statistical analysis. In the analysis, the MC method uses 50 samples and 500 samples respectively for the statistical averaging. As can be seen from Fig. 2(a) - Fig. 2(d), the calculated results of the MC method and the present method are very consistent. With the increase of the number of samples, the MC results are closer to the results of the method in this paper. For the results in Fig. 2(a), the MC (500 samples) has the maximum deviation of 9.19% and the minimum deviation of 0.02% compared with the results of the proposed method. Under the same speed condition, the calculation time of the present method is 2.23 s, compared with 74.8 s when using 100 samples and 379.3 s when using 500 samples for the MC method. It can be seen that the present method has a great computational advantage over the MC method.

In the subsequent parameter analysis of time-dependent standard deviations, it can be seen that the results of the proposed method and the MC method are also very consistent, which shows the effectiveness of the proposed method.

4.2 Different observation points

Assuming that the load moves along the track at a speed of $200\,\mathrm{km/h}$. Four observation points ($\mathrm{A}(0, 5\mathrm{m}, 0)$, $\mathrm{B}(0, 15\mathrm{m}, 0)$, $\mathrm{C}(0, 25\mathrm{m}, 0)$ and $\mathrm{D}(0, 35\mathrm{m}, 0)$) are selected to evaluate the vibration transmission characteristics.

Fig.4 - Fig. 5 show the time-dependent standard deviation and the evolutionary power spectrum of the vertical displacement response at the four observation points, respectively. Obviously, when the load moves closer to an observation point, the vibration of the observation point gradually increases; when the load passes it, the vibration of the observation point will increase rapidly; when the load starts to move away from the observation point, the vibration of the observation point will start to decrease.

The time-dependent standard deviation of the responses in Fig. 5(a) - Fig. 5(d) indicates that when the observation point is relatively close to the track, the shape of the responses curve is narrower with respect to the time axis $t = 0$ (Fig. 5(a)); on the contrary, the shape of the curve is wider relative to the time axis $t = 0$ (Fig. 5(d)). In addition, the peak value of the time-dependent standard deviation response decreases with the increasing distance from the track: the peak value of the point A is 9.2902×10^{-7}m, and the peak value of the point B is 3.1383×10^{-7}m, the peak value of the point C is 1.8279×10^{-7}m, the peak value of the point D is 1.2252×10^{-7}m. The reason for this phenomenon is that the attenuation of the vibration is related to the damping characteristics of the soil during the vibration transmission.

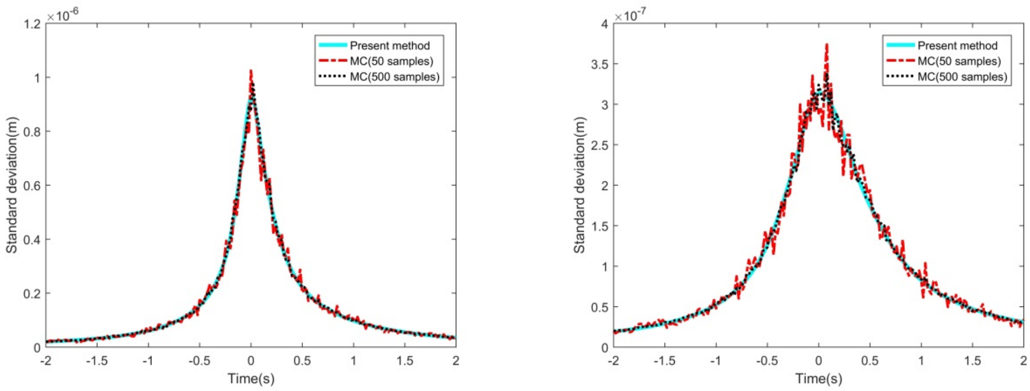

(a) $\mathrm{A}(0, 5\mathrm{m}, 0)$

(b) $\mathrm{B}(0, 15\mathrm{m}, 0)$

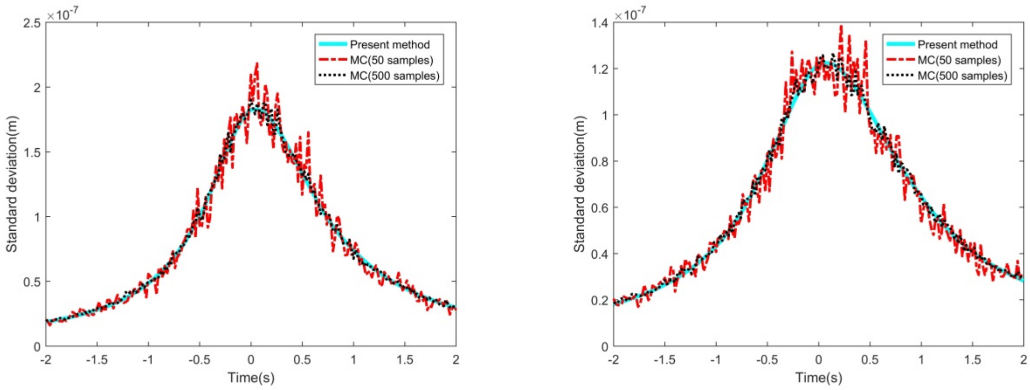

(c) $C(0, 25\mathrm{m}, 0)$ (d) $D(0, 35\mathrm{m}, 0)$

Fig. 4. Time-dependent standard deviation of vertical displacement at the different points when $v = 200\ \mathrm{km/h}$

Further, the energy distribution of the evolutionary power spectrums at different observation points is discussed. Fig. 5 shows the time-frequency distribution of the evolutionary power spectrums and its contours of the four observation points, respectively. Comparing Fig. 4(a) - Fig. 4(d), from the time axis it can be seen that when the observation point is relatively close to the track, the vibration energy is more concentrated relative to the time axis $t = 0$ (as seen at point A, Fig. 5(a1-a2)). As the distance of the observation point from the track increases, the duration of the vibration gradually becomes longer (as seen at point D, Fig.5(d1-d2)). In addition, according to the contour of the evolutionary power spectrum at each observation point, the vibration time of low frequency components gradually increases with the increase of the distance of observation point from the track (for example, the time interval of point A is $[-0.5\mathrm{s}, 0.5\mathrm{s}]$, but the time interval of point D exceeds $[-2\mathrm{s}, 2\mathrm{s}]$) and the vibration time of high-frequency components gradually decreases (for example, the frequency interval of point A is $[0, 450]\ \mathrm{rad/s}$, but the frequency interval of point D is $[0, 300]\ \mathrm{rad/s}$). The vibration characteristics of observation points at a longer distance from the track are: due to the influence of the soil damping, the vibration caused by the high-frequency component decays rapidly, the low-frequency component becomes the main contributor to the ground vibration, and the vibration duration becomes longer. In addition, the peak of the evolutionary power spectrum is flatter from Fig. 5(a1-a2) and multiple peaks appear in Fig. 5(d1-d2).

The time-dependent standard deviation of vibration response at each observation point is also computed by both the MC method and the proposed method. It can be seen from Fig. 4(a) - Fig. 4(d) that they are in good agreement. Similarly, as the number of samples increases, the result of the MC is closer to the result of the proposed method.

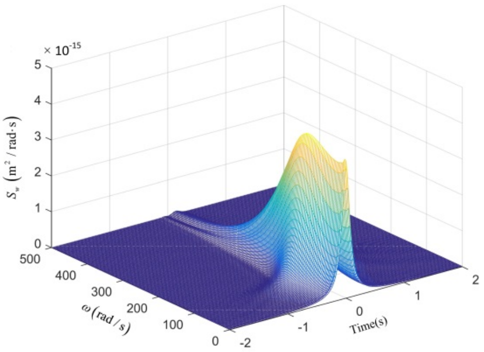

(a1) Evolutionary power spectrum of response at point A

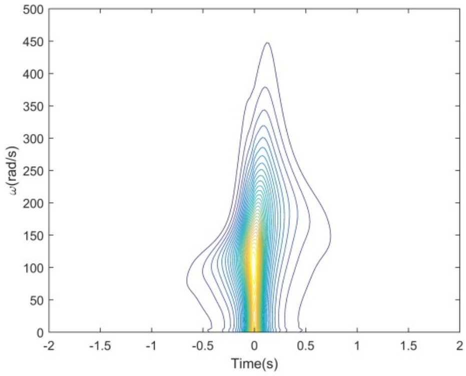

(a2) Contour of evolutionary power spectrum of response at point A

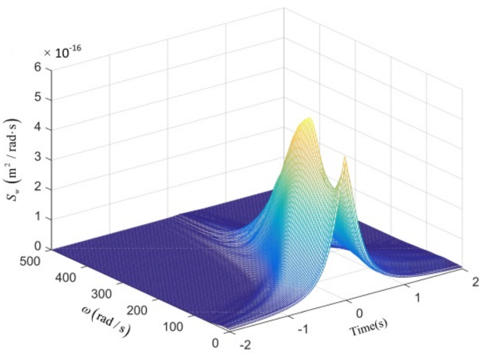

(b1) Evolutionary power spectrum of response at point B

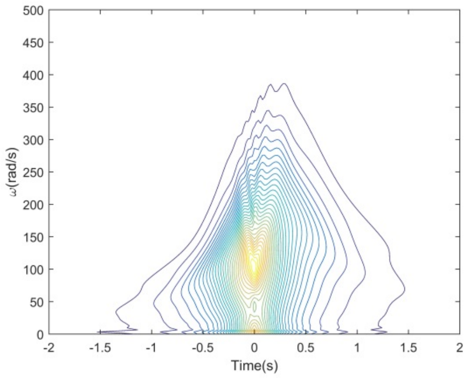

(b2) Contour of evolutionary power spectrum of response at point A

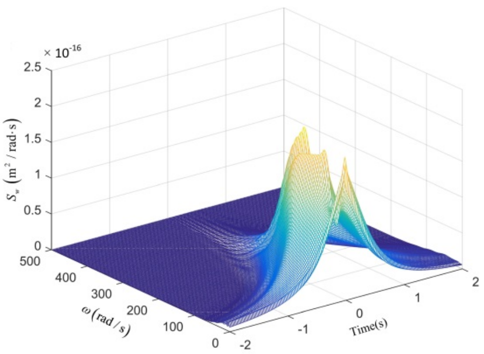

(c1) Evolutionary power spectrum of response at point C

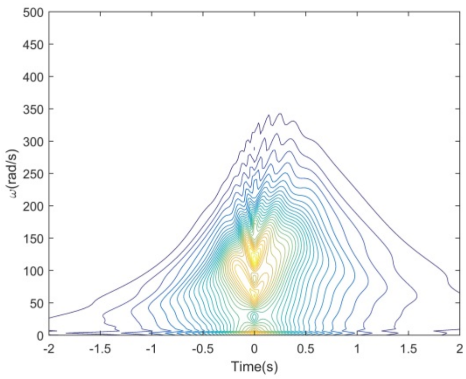

(c2) Contour of evolutionary power spectrum of response at point C

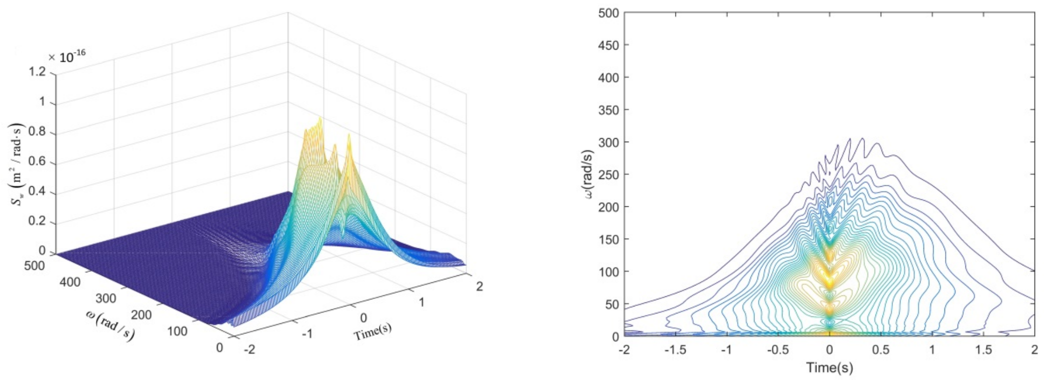

(d1) Evolutionary power spectrum of response at point D

(d2) Contour of evolutionary power spectrum of response at point D

Fig. 5. Non-stationary evolutionary power spectrum of vertical displacement at the different points when $v = 200\ \mathrm{km/h}$

4.3 Different soil characteristics

Assuming that the load moves along the track at a speed of $200\ \mathrm{km/h}$. Three kinds of the soil characteristics of Soil A, Soil B and Soil C are considered. Ground observation point $\mathrm{A}\,(0, 5\mathrm{m}, 0)$ is selected to evaluate the vibration. Fig. 6 - Fig. 7 show the time-dependent standard deviation and the evolutionary power spectrum of the vertical displacement response under the different soil parameters, respectively.

The numerical results of the time-dependent standard deviation in Fig. 6 show that the soft soil is more likely to cause greater vibration at the same speed: the peak value of the time-dependent standard deviation of soil A is $9.2902 \times 10^{-7}\mathrm{m}$ (Fig 5(a)), the peak value of the time-dependent standard deviation of soil B is $1.2700 \times 10^{-6}\mathrm{m}$ (Fig 6(b)), the peak value of the time-dependent standard deviation of soil C is $3.7816 \times 10^{-6}\mathrm{m}$ (Fig 6(c)). In addition, the response is almost symmetric with respect to the time axis $t = 0$ for harder soils A and B; whereas for soil C, the response is no longer symmetrical with respect to the time axis $t = 0$. Fig. 7 shows the evolutionary power spectrum and its contour for the response at the observation points. As can be seen from Fig. 7(a1-a2) - Fig. 7(b1-b2), for the harder soils, the frequency components of the response at the observation points are $[0{,}450]\mathrm{rad/s}$ and $[0{,}400]\mathrm{rad/s}$, respectively. For the soft soil (Fig. 7(c1-c2)), the frequency components of vibration are $[0{,}200]\mathrm{rad/s}$. Compared with the hard soil, for the vibration response of the soft soil, low frequency components play a major role.

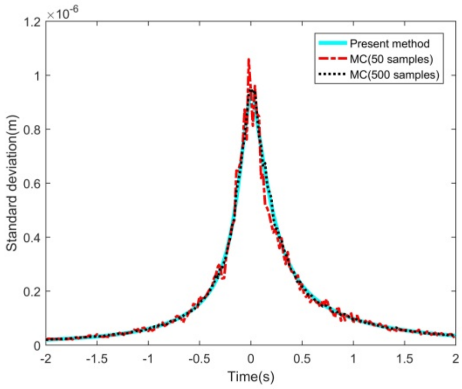

(a) Soil A

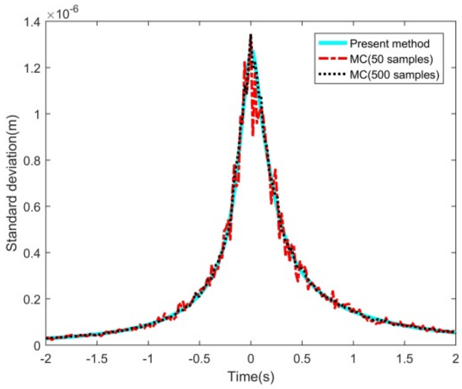

(b) Soil B

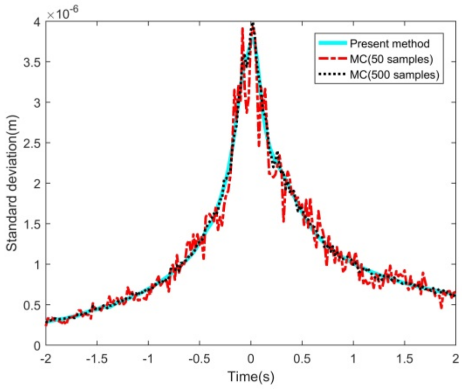

(c) Soil C

Fig. 6. Time-dependent standard deviation of vertical displacement at the A $(0, 5m, 0)$ points under different soil characteristics ($v = 200$ km/h)

As can be seen from Tab. 2, the Rayleigh wave velocity of soil C is c_{R} =92m/s. For soil C, two cases of moving load speed $v = 50\mathrm{km/h} = 13.89\mathrm{m/s} < c_{\mathrm{R}}$ and $v = 350\mathrm{km/h} = 97.22\mathrm{m/s}$ (near the value of c_{R}) are considered, respectively. The results are shown in Fig. 8. It can be seen that the energy of the vibration is mainly concentrated in the interval $[0{,}200]\mathrm{rad/s}$ (Fig. 8(a1-a2)) when the moving speed of the load is lower than the Rayleigh wave velocity ($v < c_{\mathrm{R}}$), and the energy of the vibration is concentrated in the interval $[0{,}50]\mathrm{rad/s}$ (Fig. 8(b1-b2)) when the load speed is near the Rayleigh wave velocity. The peak value of response increases with the moving velocity of the load: the peak value is $1.2847 \times 10^{-13}\ \mathrm{m^2/rad \cdot s}$ (ω =47.5799 rad/s) for $v = 50\mathrm{km/h}$; the peak value is 2.4838× $10^{-13}\ \mathrm{m^2/rad \cdot s}$ ($\omega =$ 22.3715rad/s) for $v = 200\mathrm{km/h}$; the peak value is 3.9748× $10^{-12}\ \mathrm{m^2/rad \cdot s}$ (ω =0.3142 rad/s) for $v = 350\mathrm{km/h}$. The evolutionary power spectrum analysis can visually show the vibration energy characteristics of the observation points, which has some advantages over time-domain analysis. These results suggest that for design of a high-speed rail line, the spatial characteristics of the soil would be very complex, and some measures should be taken to increase the hardness of the bearing foundation to reduce the unfavourable influence from soft soils.

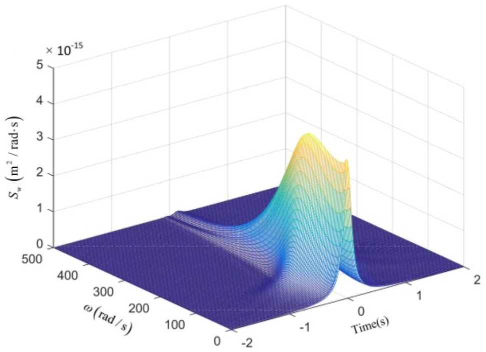

(a1) Evolutionary power spectrum of response for soil A

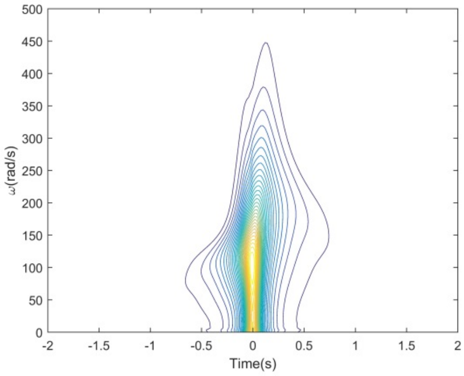

(a2) Contour of evolutionary power spectrum of response for soil A

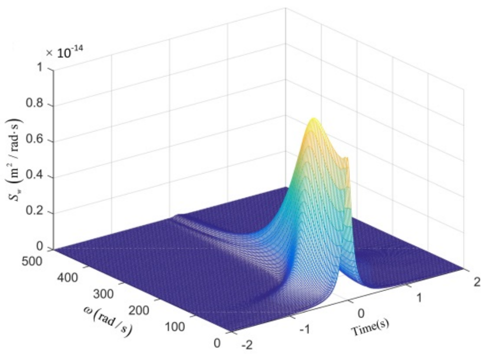

(b1) Evolutionary power spectrum of response for soil B

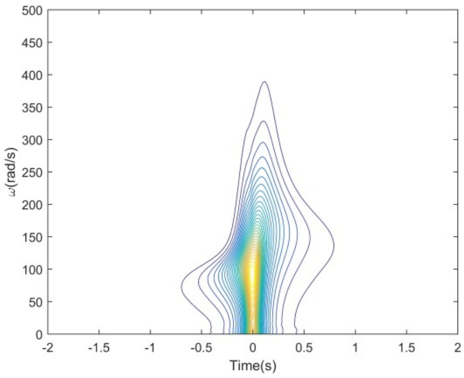

(b2) Contour of evolutionary power spectrum of response for soil B

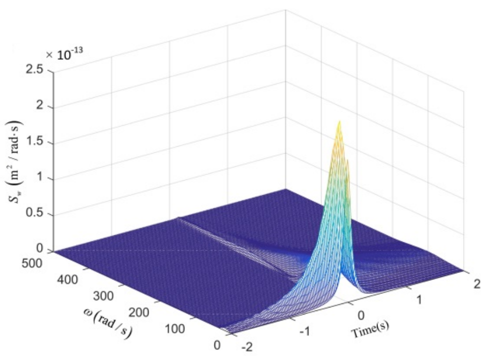

(c1) Evolutionary power spectrum of response for soil C

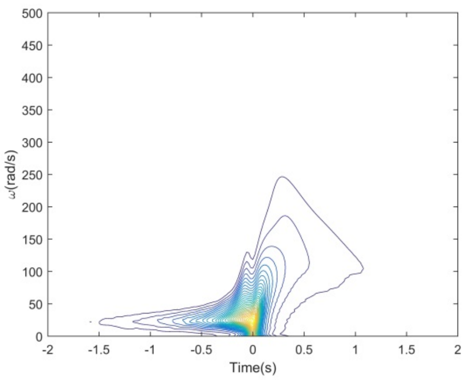

(c2) Contour of evolutionary power spectrum of response for soil C

Fig. 7. Non-stationary evolutionary power spectrum of vertical displacement at the A $(0, 5m, 0)$ points under different soil characteristics ($v = 200$ km/h)

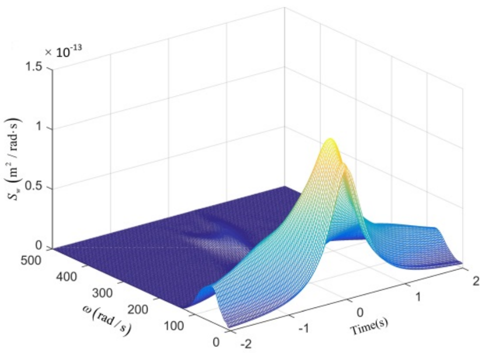

(a1) Evolutionary power spectrum when v =50km/h and Soil C

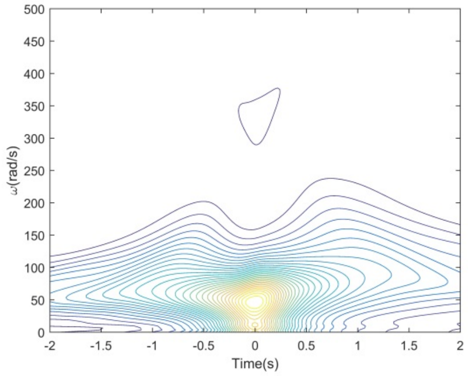

(a2) Contour of evolutionary power spectrum when v =50km/h and Soil C

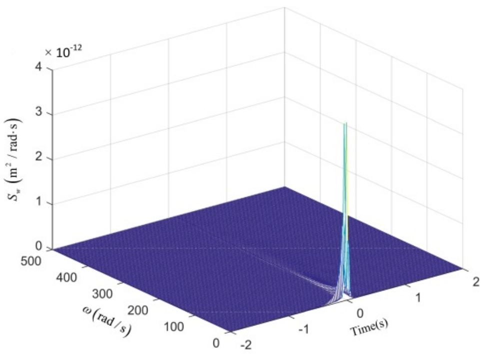

(b1) Evolutionary power spectrum when v = 350km/h and Soil C

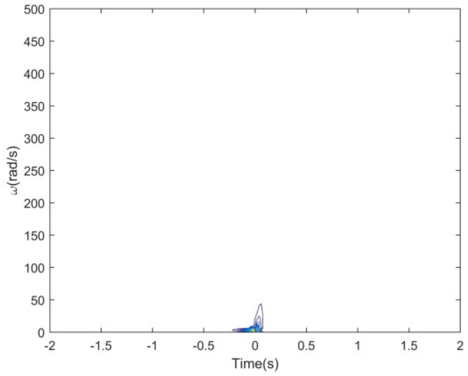

(b2) Contour of evolutionary power spectrum when v =350km/h and Soil C

Fig. 8. Non-stationary evolutionary power spectrum of vertical displacement at the A (0, 5m, 0) for different speeds

In the discussion of this section, the MC method and the proposed method are also used to compute the time-dependent standard deviation of the vibration response with the different soil characteristics of the observation point. It can be seen from Fig. 6(a) - Fig. 6(c) that the two sets of results agree well with each other.

4.4 Coherence effect of loads

When the train is running along the track, any two wheels may be considered to be subjected to the same random excitation due to the same track irregularity, but there is a certain time lag. When the two excitations are viewed at a fixed observation point, the dynamic effect of each load on the observation point is a coherence effect problem. The method proposed in this paper can also effectively analyse such problems.

In order to simulate the vehicle running on the track, four wheel-rail forces acting on the track (from four wheelsets of two bogies of a vehicle), which have time lags between them, are considered, as

$$\begin{aligned}\mathbf{f}(t) &= \{f_1(t), f_2(t), f_3(t), f_4(t)\}^{\mathrm{T}} \\ &= \{f(t-\tau_1), f(t-\tau_2), f(t-\tau_3), f(t-\tau_4)\}^{\mathrm{T}} \\ \tau_k &= \frac{(x_1 - x_k)}{v}, \quad k = 1,2,3,4\end{aligned} \tag{52}$$

in which, x_k is the relative position coordinates of the four wheel.

Considering the coherence between the loads, the pseudo excitation vector is constructed as [32] .

$$\tilde{\mathbf{f}}(t) = \sqrt{S_f(\omega)}\mathrm{e}^{\mathrm{i}\omega t}\left\{\mathrm{e}^{-\mathrm{i}\omega\tau_1}, \mathrm{e}^{-\mathrm{i}\omega\tau_2}, \mathrm{e}^{-\mathrm{i}\omega\tau_3}, \mathrm{e}^{-\mathrm{i}\omega\tau_4}\right\}^{\mathrm{T}} \tag{53}$$

Each component $\left(\sqrt{S_f(\omega)}\mathrm{e}^{-\mathrm{i}\omega\tau_k}\right)\mathrm{e}^{\mathrm{i}\omega t}$ $(k = 1,2,3,4)$ in Eq. (53) is used as an alternative to Eq. (44), and the pseudo response $\widetilde{w}_k(\mathbf{x}, \omega, t)$ $(k = 1,2,3,4)$ of the system under the pseudo excitation can be computed from Eq. (46). The evolutionary power spectrum can be compute using the following equation [32].

$$S_{ww}(\mathbf{x}, t, \omega) = \left(\sum_{i=1}^{4} \widetilde{w}_k(\mathbf{x}, \omega, t)\right)^{*} \left(\sum_{i=1}^{4} \widetilde{w}_k(\mathbf{x}, \omega, t)\right) \tag{54}$$

In Eq. (52), the relative positions of the loads to each other are respectively

$$x_1 = 0 \text{ m}, x_2 = -2.4 \text{ m}, x_3 = -18 \text{ m}, x_4 = -20.4 \text{ m} \tag{55}$$

According to Eq. (54), the nonstationary random vibration analysis of the track-soil system, in which the coherence effect of the moving loads is considered, is carried out. For the load moving along the track at speeds of $50\,\mathrm{km/h}$ and $350\,\mathrm{km/h}$, observation point A (0,0,0) is selected to evaluate the ground vibration. Fig. 9 - Fig. 10 show the time-dependent standard deviation and the evolutionary power spectrum of the vertical displacement response of point A at different velocities, respectively.

For comparison, the cases that neglect cross-correlation of the loads are also analysed. Fig. 9(a) - Fig. 9(b) show the change in the results of the standard deviation, when the cross-correlation of the wheel loads is included, is very obvious than neglect cross-correlation. When the speed is $50\,\mathrm{km/h}$, the standard deviation curve changes from the two peaks to the four peaks, but the peak value decreases. The reason for this phenomenon is that the responses of the system will be superimposed or offset by the different phases of each load. Fig. 10 - Fig. 11 show the evolutionary power spectrum at point A at velocities of $50\,\mathrm{km/h}$ and $350\,\mathrm{km/h}$, respectively, and also give the results of the same situation with and without cross-correlation of the loads. When the load speed is $50\,\mathrm{km/h}$, comparing the evolution of the power spectrums including the cross-correlation of the loads (Fig. 10(a1-a2)) with that neglecting the cross-correlation of the loads (Fig. 10(b1-b2), it can be seen that there are still four response bands, but there is no obvious equivalent contours for the results including the cross-correlation of the loads. Fig. 11 shows the evolutionary power spectrum at a load speed of $350\,\mathrm{km/h}$. A similar conclusion to the above can be reached, but due to the higher speed, there are only two response bands.

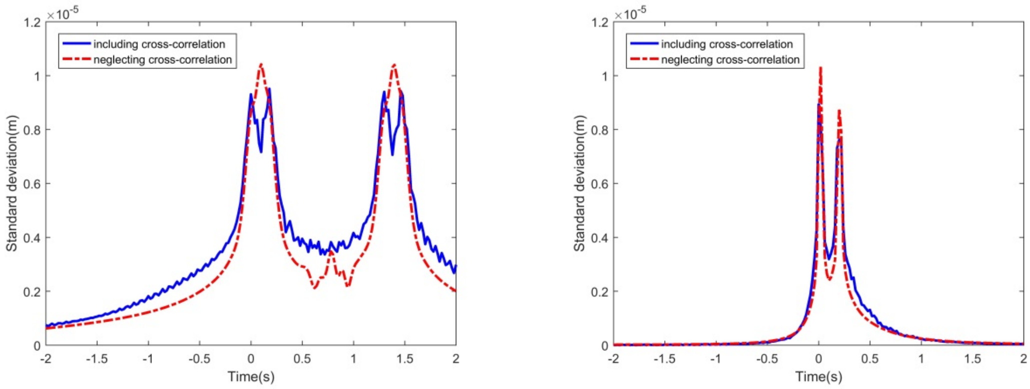

(a) v =50km/h (b) $v = 350$km/h

Fig. 9. Time-dependent standard deviation of vertical displacement at the point A (0, 0, 0) for different speeds

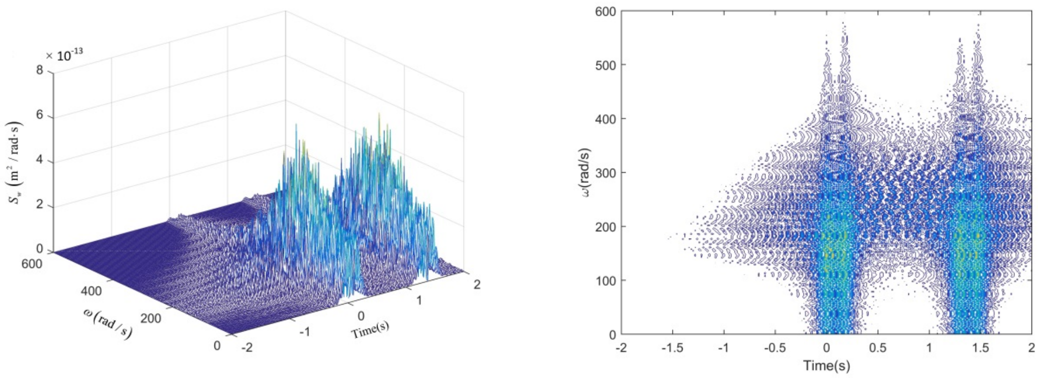

(a1) Evolutionary power spectrum including cross-correlation

(a2) Contour of evolutionary power spectrum including cross-correlation

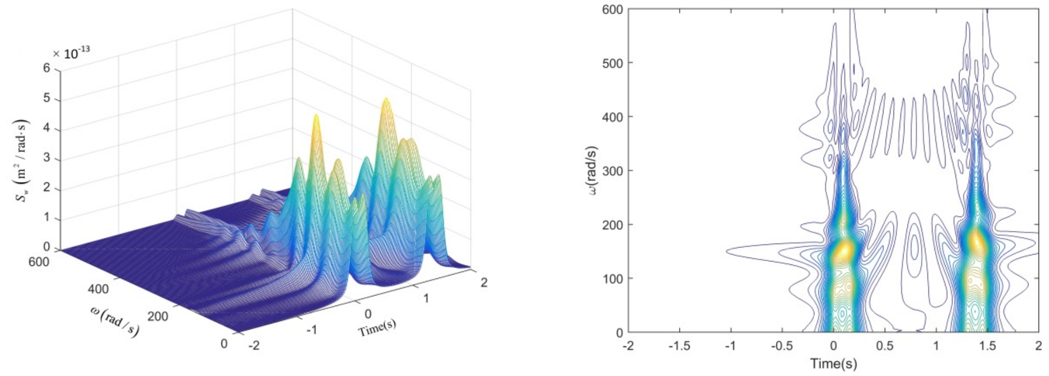

(b1) Evolutionary power spectrum neglecting cross-correlation

(b2) Contour of evolutionary power spectrum neglecting cross-correlation

Fig. 10. Non-stationary evolutionary power spectrum of vertical displacement at the point A (0, 0, 0) for v =50km/h

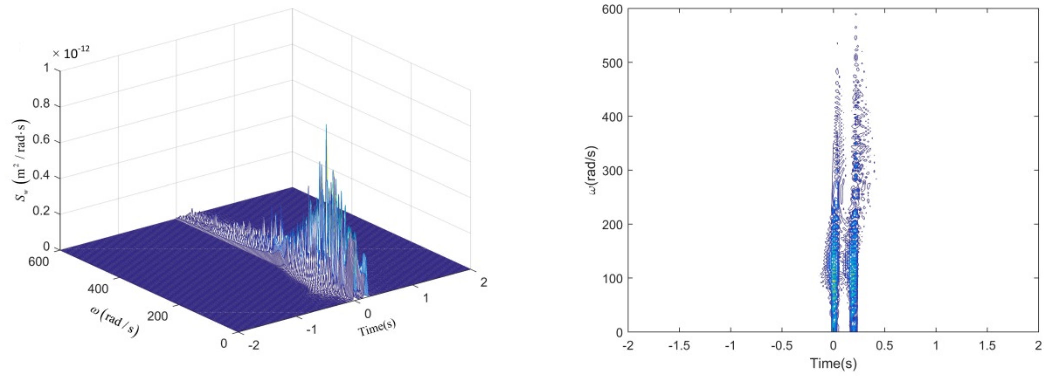

(a1) Evolutionary power spectrum including cross-correlation

(a2) Contour of evolutionary power spectrum including cross-correlation

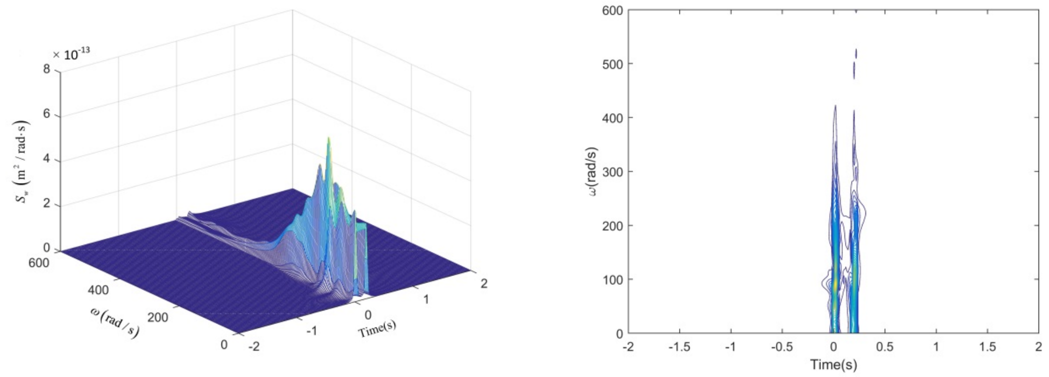

(b1) Evolutionary power spectrum neglecting cross-correlation

(b2) Contour of evolutionary power spectrum neglecting cross-correlation

Fig. 11. Non-stationary evolutionary power spectrum of vertical displacement at the point A (0, 0, 0) for v = 350km/h

5. Conclusions

A combined approach for ground vibration induced by a moving random load is proposed in this paper. The key feature of this method is to determine the coefficients of potential functions of Helmholtz equation of the soil, which is derived by decoupling the governing equations of motion for the track-soil system. The complex random ground vibration can be solved by the PEM-ITM, which is also verified by the Monte Carlo method. The presented method is proved to be very efficient and accurate.

From the detailed analysis of numerical results of the vibration responses at different parameters, the conclusions can be obtained as follows:

(1) When viewed at a fixed observation point, the train speed has a significant effect on the time-dependent standard deviation of the vibration responses of the observation point. As the speed increases, the response curve loses symmetry, while the evolutionary power spectrum response is more concentrated toward the time axis $t = 0$.

(2) At the same speed, for the different observation points, the farther away from the track, the peak value of the evolutionary power spectrum of random vibration is smaller, but the duration of vibration becomes longer, and the lower frequency components play a major role.

(3) At the same speed, soft soils have obvious vibration amplification effects. From the evolutionary power spectrum of the response, when the velocity is near the Rayleigh wave velocity, and the energy is very concentrated in the low frequency region and has very high peaks.

(4) The coherence of random loads has an obvious influence on the response of the observation point. Due to the superposition and cancellation by the individual responses from the wheel loads on the vibration of the observation point, when the cross-correlation of the loads is neglected, the curve shape of the time-dependent standard deviation of the vibration response and the peaks experience significant changes, and there is no clear borderline in the contour plot of the evolutionary power spectrum.

Acknowledgements

The authors are grateful for support under grants from the National Basic Research Program of China (2014CB046803) and the National Science Foundation of China (11772084).

References

1. Zhou, S., He C., Di, H. et al.: An efficient method for predicting train-induced vibrations from a tunnel in a poroelastic half-space. Engineering Analysis with Boundary Elements, 2017, 85:43-56. Engineering Analysis with Boundary Elements, **85**:43-56 (2017)
2. Li, G.Q., Wang, Z.L.,Chen, S. et al.: Field measurements and analyses of environmental vibrations induced by high-speed Maglev. Science of the Total Environmen. **568**:1295-1307 (2016)
3. Fryba, L.: Vibration of solids and structures under moving loads. Springer Science & Business Media (2013)
4. Alabi, B.: A Parametric Study on Some Aspects of Ground-Borne Vibrations Due to Rail Traffic. J Sound Vib. **153**, 77-87 (1992)
5. Krylov, V.: Generation of Ground Vibrations by Superfast Trains. Appl Acoust. **44**, 149-164 (1995)
6. Takemiya, H., Goda K.: Prediction of ground vibration induced by high-speed train operation. Proceedings of the 18th Sino-Japan Technology Seminar. 1-10 (1997)
7. Gunaratne, M., Sanders, O.: Response of a layered elastic medium to a moving strip load. Int J Numer Anal Met. **20**, 191-208 (1996)
8. Dieterman, H., Metrikine, A.: Critical velocities of a harmonic load moving uniformly along an elastic layer. J Appl Mech. **64**, 596-600 (1997)
9. Lefeuve-Mesgouez, G., Peplow, A.T., Le Houédec, D.: Surface vibration due to a sequence of high speed moving harmonic rectangular loads. Soil Dyn Earthq Eng. **22**, 459-473 (2002)
10. Jones, C.J.C., Sheng, X., Petyt, M.: Simulations of ground vibration from a moving harmonic load on a railway track. J Sound Vib. **231**,739-751 (2000)
11. Bierer, T., Bode, C.: A semi-analytical model in time domain for moving loads. Soil Dyn Earthq Eng. **27**, 1073-1081 (2007)
12. Sheng, X., Jones, C.J.C., Petyt, M.: Ground vibration generated by a harmonic load acting on a railway track. J Sound Vib. **225**, 3-28 (1999)
13. Hung, H.H., Yang, Y.B.: Elastic waves in visco-elastic half-space generated by various vehicle loads. Soil Dynamics and Earthquake Engineering. **21**, 1-17 (2001)
14. Koziol, P., Mares, C., Esat, I.: Wavelet approach to vibratory analysis of surface due to a load moving in the layer. Int J Solids Struct. **45**, 2140-2159 (2008)
15. Sheng, X., Jones, C.J.C., Thompson, D.J.: A comparison of a theoretical model for quasi-statically and dynamically induced environmental vibration from trains with measurements. J Sound Vib. **267**, 621-635 (2003)
16. Lombaert, G., Degrande, G.: Ground-borne vibration due to static and dynamic axle loads of InterCity and high-speed trains. J Sound Vib. **319**, 1036-1066 (2009)

17. Xia, H., Cao, Y.M., De Roeck, G.: Theoretical modeling and characteristic analysis of moving-train induced ground vibrations. J Sound Vib. **329**, 819-832 (2010)
18. Hunt, H.: Modelling of road vehicles for calculation of traffic-induced ground vibration as a random process. J Sound Vib. **144**, 41-51 (1991)
19. Sun, L., Greenberg, B.S.: Dynamic response of linear systems to moving stochastic sources. J Sound Vib. **229**, 957-972 (2000)
20. Metrikine, A., Vrouwenvelder, A.: Surface ground vibration due to a moving train in a tunnel, two-dimensional model. J Sound Vib. **234**, 43-66 (2000)
21. Paolucci, R., Maffeis, A., Scandella, L., et al.: Numerical prediction of low-frequency ground vibrations induced by high-speed trains at Ledsgaard. Sweden. Soil Dyn Earthq Eng. **23**, 425-433 (2003)
22. Sheng, X., Jones, C., Thompson, D.: A theoretical model for ground vibration from trains generated by vertical track irregularities. J Sound Vib. **272**, 937-965 (2004)
23. Lai, C.G., Callerio, A., Faccioli, E., et al.: Prediction of Railway-Induced Ground Vibrations in Tunnels. J Vib Acoust. **127**, 503-514 (2005)
24. Lin, J.H.: A fast CQC algorithm of PSD matrices for random seismic responses. Comput Struct. **44**, 683-687 (1992)
25. Lu, F., Gao, Q., Lin, J., et al.: Non-stationary random ground vibration due to loads moving along a railway track. J Sound Vib. **298**, 30-42 (2006)
26. Lombaert, G., Degrande, G., Clouteau, D.: Numerical modelling of free field traffic-induced vibrations. Soil Dyn Earthq Eng. **19**, 473-488 (2000)
27. Bendat, J. S., Piersol, A. G.: Random data: analysis and measurement procedures. vol. 729. John Wiley & Sons (2011)
28. Peng, Y.B., Chen, J.B., Li, J.: Nonlinear Response of Structures Subjected to Stochastic Excitations via Probability Density Evolution Method. Advances in Structural Engineering. **17**, 801-819 (2014)
29. Zhang, Y.W., Zhao, Y., Zhang, Y.H., et al.: Riding comfort optimization of railway trains based on pseudo-excitation method and symplectic method. Journal of Sound & Vibration.**332**, 5255-5270 (2013)
30. Zhao, G.Z., Chen, G., Zhan, K. et al.: An iterative algorithm for analysis of coupled structural–acoustic systems subject to random excitations. Acta Mechanica Sinica. **28**, 458-467 (2011)
31. Liu, S.T., Lin, Z.Q., Gea, H.C.: Design of piezoelectric energy harvesting devices subjected to broadband random vibrations by applying topology optimization. Acta Mechanica Sinica. **27**, 730-737 (2011)
32. Zhao, Y., Si, L.T., Ouyang, H.: Dynamic analysis of an infinitely long beam resting on a kelvin foundation under moving random loads. Shock and Vibration. **2017**,1-13 (2017)